PAPER

Check for updates

Sustainable water-activated metal–air paper batteries based on waste biomass-based electrocatalysts†

Kosuke Ishibashi and Hiroshi Yabu [ID] *

In this study, we synthesized a biomass-derived carbon alloy catalyst, termed "nano-blood charcoal (NBC)," using dried blood meal and cellulose nanofibers (CNFs) sourced from sea pineapple shells. This catalyst demonstrated high activity under neutral conditions and enabled the successful fabrication of a high-output, environmentally friendly water-activated magnesium–air paper battery. The open circuit voltage (OCV) of the cell was 1.57 V, and the maximum current density was 161 mA cm^{-2}. The maximum power density was 55.7 mW cm^{-2}, and the capacity of a single paper battery cell was 749 mW h g$_{(Mg)}^{-1}$. Additionally, the oxygen evolution reaction (OER) performance of NBC was also evaluated, and it contributed to realize a rechargeable Mg–air paper battery.

Sustainability spotlight

Batteries produce harmful wastes and CO_2 emissions during their production and disposal. Metal–air batteries use precious metals and heavy metals as electrode catalysts and current collectors. Although hetero-atom-doped carbon alloys are attracting attention as alternative materials for cathode electrode catalysts, concerns about sustainability arise because these materials are made by petroleum or mineral resources. We used discarded sea-pineapple shells and dried blood powder as raw materials for carbon alloy catalysts. By pyrolyzing these materials, we successfully synthesized highly active electrode catalysts and achieved a high-power, high-capacity magnesium–air paper battery. This achievement not only enables the creation of high-performance batteries but also promotes resource recycling by utilizing waste, contributing to sustainable battery technology.

Introduction

A metal–air paper battery, which generates electricity when the paper absorbs saline or other solutions, is attracting attention as an emergency power source, a device for sensing moisture, and a lightweight energy source for wearable devices.[1,2] A zinc–air paper battery using zinc powder as the anode and the cathode is printed on the paper,[3] and metal–air paper batteries using magnesium,[4] which easily dissolves in neutral water, have been reported. However, these metal–air paper batteries have had issues such as limited device applicability due to their low output power densities and the use of environmentally harmful or precious materials, like manganese and silver paste, as catalysts or electrodes. Therefore, there has been a demand for metal–air paper batteries that are environmentally friendly and safe and have high-power output.

The output power of metal–air batteries depends on the efficiency of the oxygen reduction reaction (ORR) at the cathode. By using a cathode with a catalyst with high ORR activity, it is possible to reduce the reaction overvoltage and achieve a high-output paper battery. Precious metal catalysts, like Pt/C, are known to show high activity as ORR catalysts,[5–8] but they have issues regarding environmental impact and safety. On the other hand, we have succeeded in creating a high-performance metal–air paper battery using low-environmental-impact and safe materials based on single-atom catalysts, including metal phthalocyanines, their derivatives, and carbon alloys prepared by pyrolysis of metal complexes.[9–11]

In recent years, synthesizing electrochemical catalysts from waste biomass-derived materials has also been examined. Carbon alloys that introduce metal complex structures, like nitrogen or FeN_4, into carbon show high activity as ORR catalysts. Studies have been reported on obtaining carbon alloy catalysts by carbonizing materials derived from waste biomass.[12–17] Recently, we have reported that by mixing cellulose nanofibers derived from tunicate shells, which are discarded as industrial waste, and dried blood powder, a waste biomass generated during meat processing, and then pyrolyzing them, a carbon alloy, named nano-blood charcoal (NBC) with high ORR catalyst activity under alkaline conditions could be obtained.[18] In this process, the heme iron contained in the dried blood powder acts as a catalytic active site, and the cellulose from tunicate shells provides high conductivity and catalytic

Advanced Institute for Materials Research (WPI-AIMR), Tohoku University, 2-1-1, Katahira, Aoba-Ku, Sendai 980-8577, Japan. E-mail: hiroshi.yabu.d5@tohoku.ac.jp
† Electronic supplementary information (ESI) available. See DOI: https://doi.org/10.1039/d4su00607k

Paper

activity upon carbonization. Furthermore, by mixing cobalt complexes, like vitamin B_{12}, we have successfully synthesized NBC that introduces iron–cobalt complex sites into the carbon framework, exhibiting both high ORR activity and OER/HER activity under alkaline conditions.[19]

However, to apply biomass-derived carbon alloy catalysts to the previously mentioned magnesium paper–air batteries, an ORR catalyst that shows high activity in neutral electrolytes such as saline is required. Therefore, in this study, we evaluated the ORR performance of NBC catalysts in neutral conditions. Using this catalyst, we successfully fabricated a high-output, low-environmental-impact magnesium paper–air battery and demonstrated that it can be used as a power source for various wearable devices.

Experimental

Materials

Mg foil ($0.03 \times 100 \times 100$ mm) was purchased from NIRACO, Co., Ltd (Tokyo, Japan). The Mg sheet ($100 \times 300 \times 0.2$ mm) was purchased from AS One Corporation (Osaka, Japan). Dimethyl sulfoxide (DMSO), isopropyl alcohol (IPA), and other solvents were purchased from Fujifilm Wako Chemical Industry, Inc. (Osaka, Japan). Cellulose nanofiber (CNF), which was extracted from sea pineapple shells, was purified according to the literature.[18] Blood meals were kindly provided by Tomikura Sangyo and powdered by a jet mill. Multi-layer CNT with a diameter of 20–60 nm and length of 0.5–2.0 mm was purchased from Koatsu Gas Kogyo. Styrene-butadiene rubber (SBR) binder (AL-1002) was purchased from Nippon A&L, Inc., Osaka, Japan.

Synthesis of carbon alloy catalysts

The preparation process of carbon alloy catalysts is shown in Fig. 1. The powdered BM and CNFs were mixed in various weight ratios by hand grinding in water, and the resultant mixtures were dried at room temperature *in vacuo*. In order to avoid those heterogeneities, we mixed, ground and homogenized the samples before pyrolysis. It is important to mix BM powders with CNFs in the nanoscale to realize carbons with atomically doped heteroatoms. If those two materials were not mixed well, the obtained NBC comprises a mixture of carbons

Fig. 1 Preparation process of NBC catalysts from waste biomass resources.

from CNFs and pyrolyzed BMs. To realize the single-atom doped carbons, such heterogeneity should be avoided. This is the reason why we mixed and ground to homogenize the raw materials. The pyrolyzed samples were derived from the same crude materials after mixing and grinding, therefore, we considered that there are no intended heterogeneities. The dried samples were pyrolyzed in an electric oven at 900 °C *in vacuo* for 2 h. The heating rate was 20 °C min^{-1}. After pyrolysis, the sample was slowly cooled to room temperature. After this pyrolysis process, powder-like carbon alloys were obtained.

Characterization of synthesized carbon alloys

The surface morphologies and elemental mapping of the sample electrodes were observed using an electron probe micro analyzer (EPMA, JXA-8530F, JEOL, Tokyo, Japan).

Electrochemical measurements

The ORR performance was evaluated by linear-sweep voltammetry (LSV) measurements using a potentiostat (2325, BAS, Japan). Catalyst inks for each sample were prepared by dispersing 0.82 mg of the catalyst in a 1 mL solution consisting of 6 μL Nafion (527084, Sigma-Aldrich, USA), 33 μL isopropyl alcohol, and 84 μL water *via* sonication for 5 min. Twenty microliters of the ink were then cast onto a glassy carbon (GC, BAS, Japan) insert of a rotating ring-disk electrode (RRDE; 4 mm diameter, BAS, Japan) and dried. The catalyst loading on the electrode was 300 μg cm^{-2}. A Pt wire and an Ag/AgCl electrode were inserted into the electrolyte as reference and counter electrodes, respectively. A 0.1 M KOH solution bubbled with N_2 or O_2 for 30 min was used as the electrolyte. In addition, 3 M methanol was added to an O_2-saturated 0.1 M KOH solution for evaluation of the methanol oxidation activity of the catalysts. The potential *vs.* Ag/AgCl was converted to the reversible hydrogen electrode (RHE) scale using the following equation:

$$E(vs.\ \text{RHE}) = E(vs.\ \text{Ag/AgCl}) + 0.197 + 0.059\ \text{V} \times \text{pH} \quad (1)$$

The number of electrons (n) involved in the ORR was calculated according to the Koutecký–Levich (K–L) equation:[20]

$$\frac{1}{J} = \frac{1}{J_k} + \frac{1}{J_d} = \frac{1}{nFAkC_{O_2}} + \frac{1}{0.62nFAD_{O_2}^{2/3}\nu^{-1/6}C_{O_2}\omega^{1/2}} \quad (2)$$

where J, J_k, and J_d are the measured, kinetic, and diffusion-limiting current, respectively; F is the Faraday constant (96 485 C mol^{-1}); A is the electrode area (0.1256 cm^2); k is the rate constant for oxygen reduction (M s^{-1}); D_{O_2} is the diffusion coefficient of O_2 in the electrolyte (1.93×10^{-5} cm^2 s^{-1}); ν is the viscosity of the electrolyte solution ($1.009 \times 10^-$ cm^2 s^{-1}); C_{O_2} is the saturated concentration of O_2 in the electrolyte (1.26×10^{-6} mol cm^{-1}); and ω is the angular rotation rate.

The number of electrons n involved in the ORR was also calculated using the RRDE results and the following equation:
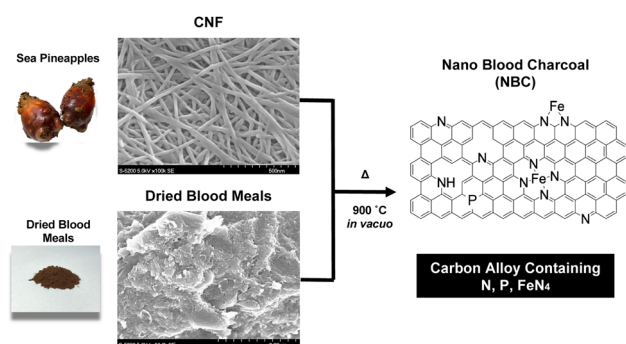
$$n = \frac{4I_D}{I_D + \dfrac{I_R}{N}} \quad (3)$$

where I_D and I_R are the current densities of the disk and ring electrodes, respectively, and N is the capture efficiency (0.42).

Mg–air paper battery cells

Fig. 2 shows a schematic illustration of a paper battery cell.[21] Catalyst ink containing 100 mg of NBC or MnO$_2$/Vulcan, SBR binder, and carbon fibre mixture (mixing ratio was 40 : 20 : 40) in 4 mL IPA was prepared. The catalyst ink was coated on a paper sheet and formed a 10 mm × 10 mm cathode. A Mg foil, three stacks of paper sheets, and the catalyst-coated paper sheet were stacked and fixed with plastic clips at the side. Current–voltage (I–V), current–power (I–P), and discharge polarization curves of the paper battery cells were measured by using potentiostat (VersaSTAT 4, Ametek, US) after absorbing 4.0 M NaCl aq.

Results and discussion

Characterization

The obtained NBC catalysts coated on a paper sheet were investigated using EPMA and XPS. Fig. 3 presents cross-sectional SE and elemental mapping images of the NBC catalyst-coated paper sheet measured by EPMA. From the SE image, there is a clear contrast between the paper and the catalyst layer. The interface between those two layers is shown as a red dashed line. Elemental mapping image of C (Fig. 3(b)) and O (Fig. 3(c)), the contrasts between those two layers are clearly observed in the elemental mapping of C and O. This was caused by the difference between C and O contents between paper and NBC. Paper is mainly composed of cellulose fibers. Cellulose is a polysaccharide whose chemical formula is $(C_6H_{10}O_5)_n$. Therefore, the paper contains 44.4% of carbon and 49.3% of oxygen. On the other hand, NBC is composed of mainly pyrolyzed carbon networks. Therefore, stronger carbon signals were obtained from the catalytic layer than the paper region (Fig. 3(b)), and the signal intensity was inverted in the
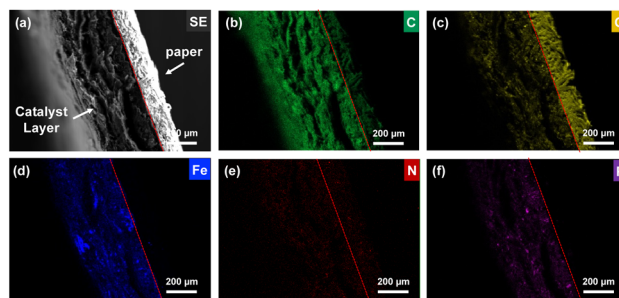

Fig. 3 Cross-sectional EPMA measurement results of the catalyst layer coated paper. A SE (a) image, and elemental mapping images of C (b), O (c), Fe (d), N (e), and P (f) are shown. Red dashed line in each image shows an interface between the paper and the catalyst layer.

elemental mapping of oxygen (Fig. 3(c)). The results indicated that the NBC catalyst had high C content and low O content compared with the paper, which implies the formation of a carbon network from CNFs in the NBC catalyst. Elemental mapping images of Fe, N, and P indicate that those elements were successfully incorporated into the carbon network (Fig. 3(d)–(f)). Those heteroatom elements were derived from dried blood meals.

The wide and narrow scan XPS spectra of the NBC catalyst are shown in Fig. 3. In the wide scan XPS spectrum (Fig. 4(a)), distinct peaks corresponding to C$_{1s}$, O$_{1s}$, and O$_{KLL}$ were observed, alongside minor peaks attributed to Ca$_{2s}$, Ca$_{2p_{3/2}}$, Na$_{1s}$, Na$_{KLL}$, P$_{2s}$, P$_{2p_{3/2}}$, and N$_{1s}$. The Na and Ca peaks originated from contamination by mineral resources present in the sea pineapple shells and blood meals, while phosphate was
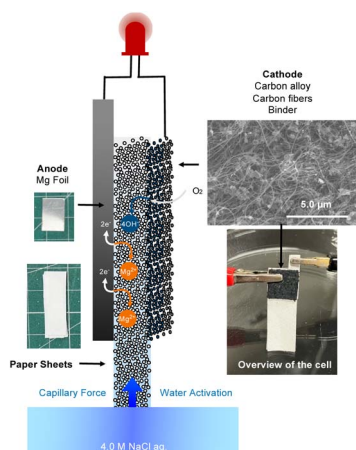

Fig. 2 Schematic of a Mg–air paper battery cell. The inset images on the left side show each component of the anode and paper sheets, and the right side images show an overview of the cell and the SEM image of the cathode, respectively.
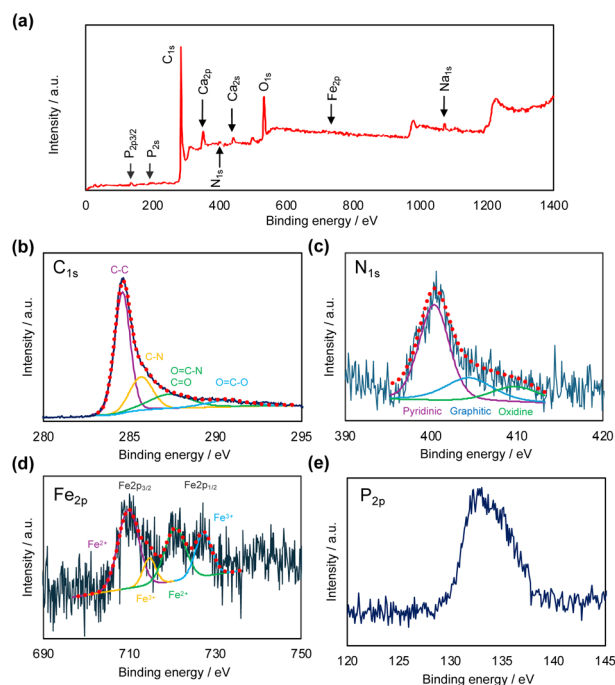

Fig. 4 Wide scan (a) and narrow scan of C$_{1s}$ (b), N$_{1s}$ (c), Fe$_{2p}$ (d), and P$_{2p}$ (e) XPS spectra of NBC. The inset spectra in (b)–(d) show waveform separation of components.

introduced from lipids in the blood meals. Fig. 4(b) displays the narrow scan of the C_{1s} peak at 285 eV, which, through the waveform separation, revealed multiple peaks associated with C–C, C=O, and C–N, suggesting the formation of various bonds during the pyrolysis process. By waveform separation of the narrow scan of the N_{1s}, the peaks were attributed to pyridinic N, graphitic N, and oxide N at 399 eV, 403 eV, and 408 eV, respectively (Fig. 4(c)).[22] Fe peaks (Fig. 4(d)) indicated that $Fe_{2p_{3/2}}$ and $Fe_{2p_{1/2}}$ of Fe(II) and Fe(III) were found. Those results strongly support the existence of the FeN_4 structure within the carbon network. As shown in Fig. 4(e), $P_{2p_{3/2}}$ is clearly observed, which indicates incorporation of phosphorous group in the carbon network.

RRDE measurements

The ORR performance of the synthesized carbon alloy was evaluated using a rotating ring-disk electrode (RRDE). MnO_2 and glassy carbon (GC) were also tested as reference materials. Fig. 5(a) shows the LSV curves measured at both the ring and disk electrodes for the carbon alloy, MnO_2/Vulcan, and GC in O_2-saturated 1 M NaCl aqueous solution at a rotating speed of 1600 rpm. The LSV curves of GC showed a lower disk current and higher ring current in the low potential region, indicating poor ORR performance. In the case of MnO_2/Vulcan, an onset

Fig. 5 LSV curves for ORR on ring and disc electrode at its rotating speed of 1600 rpm (a), H_2O_2 production rate (b) of GC, MnO_2/Vulcan, and NBC, rotating speed dependence of LSV curves (c), and K–L plot of NBC (d), LSV curves for OER (e), and LSV curves for ORR/OER bifunctional property (f).

potential (E_{onset}) and a half-wave potential ($E_{1/2}$) were 0.50 V vs. RHE and 0.40 V vs. RHE, respectively. A maximum current density of -4.0 mA cm^{-2} from the ring current indicated H_2O_2 production, but it was notably suppressed compared to that of GC. On the other hand, the NBC demonstrated a higher E_{onset} (0.80 V vs. RHE) and $E_{1/2}$ (0.53 V vs. RHE). The maximum current density value was almost the same as that of MnO_2/Vulcan. While typical ORR catalysts such as MnO_2 exhibit low ORR activity under neutral conditions, the NBC derived from waste biomass showed superior ORR performance.

In order to decide the suitable composition, we evaluated NBCs derived from different mixing ratios of BM powders and CNFs. In the ESI, S1,† Fig. S1† shows LSV curves of NBCs derived from different mixing ratios of BM powders and CNFs and MnO_2/Vulcan in 1 M NaCl aq. at the ring-disc electrode rotating speed of 1600 rpm. The onset potentials of NBCs were higher than those of MnO_2/Vulcan, however, there were some variations in NBCs. In terms of the onset potential, which is one of the important factors of ORR activity, and conductivity, the NBC derived from BM powders:CNFs = 5:5 had the highest performance. When the content of BM powders was low and CNF content was high, the number of catalytic sites decreased because the heteroatom content became lower. In contrast, the conductivity decreased with increasing BM powders and decreasing CNF contents. The best balance of BM powders and CNFs is required to achieve both high ORR catalytic properties and high conductivity. This is the reason why we chose this composition.

The ORR process consists of two main pathways: the 4-electron pathway, in which two O_2 molecules are converted into four water molecules, and the 2-electron pathway, which leads to H_2O_2 generation. The ratio of H_2O_2 production reflects the balance between these two pathways. Fig. 4(b) shows the H_2O_2 production rate of each electrode, which is calculated from the ring and disc currents. At all potential regions, the plot indicates that GC had high H_2O_2 generation, while MnO_2 and the NBC significantly suppressed H_2O_2 production, suggesting that the 4-electron pathway was the dominant ORR mechanism.

LSV curves were also measured at various rotating speeds (Fig. 5(c)). From the results, Koutecký–Levich (K–L) plots for NBC were plotted according to eqn (2) (Fig. 5(d)) and it was determined that the electron numbers of ORR ranged from 3.46 to 3.79, which supports that the ORR on NBC catalyst proceeded mainly through a 4-electron process. These numbers were much higher than those of the MnO_2/Vulcan case (3.23–3.32, see ESI, S2†). The BM contains not only hemoglobin but also proteins and phospholipids in large amounts, with only trace amounts of iron. Therefore, the introduction of iron into the obtained carbon was minimal. On the other hand, it is noteworthy that high catalytic activity was achieved even with such a small amount of iron indicating that not only the highly active FeN_4 structure for ORR but also other heteroatoms such as nitrogen and phosphorus contribute to the catalytic activity.

The current in the ORR curve does not reach the saturation level, and it increases with the lowering of the potential. The saturation limit at ORR activity strongly depends on the reactive surface area of the catalyst. MnO_2/Vulcan had a lower relative
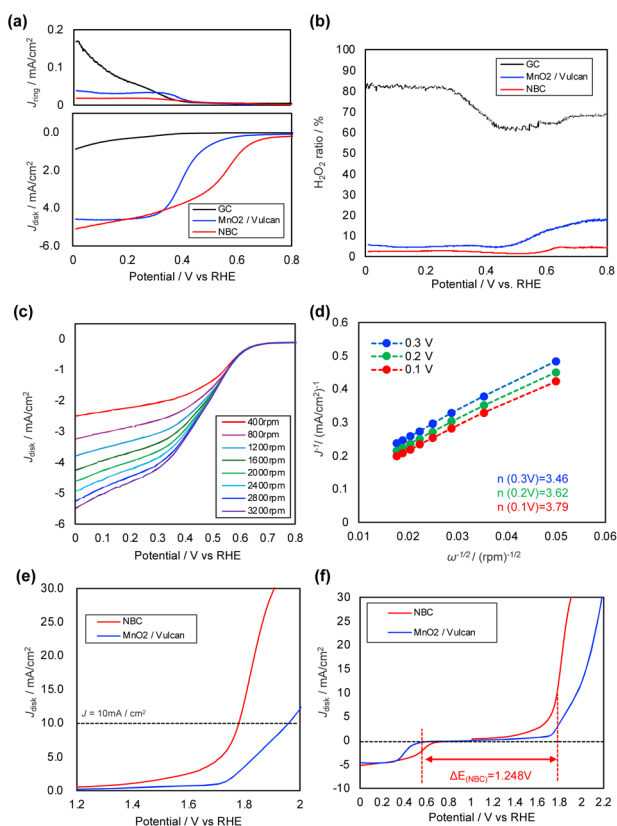
surface area than other carbons, such as Ketjen black, which means that the number of active sites was quite limited. Therefore, the MnO$_2$/Vulcan reached the saturation limit at the lower potential region. On the other hand, the NBC was derived from CNFs, which had nanoscale fiber structures, that resulted in highly porous structures. This porous structure enlarges the reactive surface areas of NBCs. This is the reason why the current density increases with decreasing the potential value.

It is noteworthy that NBC also has oxygen evolution reaction (OER) catalytic property. In the previous work, we found bifunctional electrocatalytic properties of NBC both for ORR and for OER under alkaline conditions,[18] however, no work has been reported indicating OER performance under neutral conditions. Fig. 5(d) shows LSV curves for OER of NBC and MnO$_2$/Vulcan. From the potential value at 10 mA cm^{-2} ($E_{j=10mA\,cm^{-2}}$), the values of NBC and MnO$_2$/Vulcan were 1.78 V *vs.* RHE and 1.96 V *vs.* RHE, respectively. The results showed that NBC had much higher OER performance than MnO$_2$/Vulcan.

Fig. 5(f) showed that ORR/OER bifunctional properties of NBC and MnO$_2$/Vulcan. The values ΔE ($E_{j=10mA\,cm^{-2}} - E_{1/2}$) of NBC and MnO$_2$/Vulcan were 1.25 V and 1.56 V, respectively. Those results indicate that NBC has good ORR/OER bifunctional properties.

Mg–air paper battery cells

From the RRDE measurements, the NBC catalyst synthesized from waste biomass resources had high ORR activity in a neutral electrolyte condition. To apply this property for realizing a high-performance magnesium–air paper battery cell, the carbon alloy was mixed with carbon fibers, SBR binder, and dispersed in IPA, and then coated on a paper sheet. A paper battery cell was fabricated according to the literature.[21]

The inset images of Fig. 5(a) show a photograph of the cell and a SEM image of the cathode. The cell was fabricated only by stacking a Mg foil, paper for water absorption, and cathode coated on paper. As shown in the SEM image of the cathode, particulate carbon alloy electrocatalysts and carbon fibers were fixed with SBR binders.

Fig. 6(b) shows current density–voltage (*I–V*) and current density–power density (*I–P*) polarization curves of the fabricated Mg–air paper battery cells activated by salt water. The open circuit voltage (OCV) of the cell was 1.57 V and the maximum current density was 161 mA cm^{-2}. The maximum power density was 96.8 mW cm^{-2} using NBC. However, the OCV, the maximum current density, and power density of the cell using MnO$_2$/Vulcan were 1.50 V, 102 mA cm^{-2}, and 55.3 mW cm^{-2}, respectively. From these results, the Mg–air paper battery cell using NBC had superior performance compared with the MnO$_2$/Vulcan case. It is noteworthy that the cathode had enough electronic conductivity without using a current collector and the maximum output power density was almost identical to the case using other cutting-edge electrocatalysts for Mg–air paper battery.

Fig. 6(c) shows the discharge polarization curves of the cell. The discharging time of the cell after activation by salt water continues for over 2 hours at 10 mA cm^{-2}. From the result, the
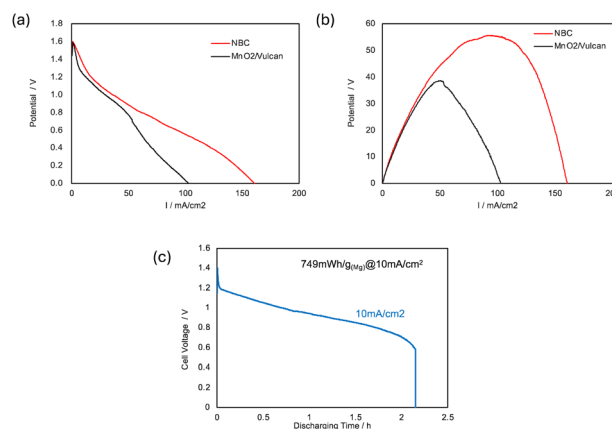

Fig. 6 *I–V*/*I–P* polarization curves of the cell using NBC or MnO$_2$/Vulcan as cathode catalysts (a and b), and discharge polarization curves of the cell using NBC as a cathode catalyst (c).

total capacity of a single paper battery cell was 749 mW h g$_{(Mg)}^{-1}$.

Rechargeable Mg–air paper battery cells

Application of the Mg–air paper battery cell using biomass-derived electrocatalysts for a rechargeable battery is very challenging and to the best of our knowledge, there is no report about the realization of rechargeable Mg–air paper battery, which uses neutral electrolytes such as salt water. The OER measurement of the NBC showed good OER performance even in the neutral condition. The Mg–air paper battery uses neutral saline as the electrolyte. OER has higher reaction efficiency in acidic or alkaline environments, and highly active OER catalysts are well-known under such conditions. However, there has been very little investigation into highly active OER catalysts near neutral pH. Without an effective catalyst, the charging overpotential becomes large, raising concerns about the evaporation of the electrolyte due to heat, damage to the electrodes and paper, and in the worst case, the risk of fire. To avoid these issues, an OER catalyst that efficiently reduces the charging overpotential is necessary. The newly developed NBC has higher OER activity than MnO$_2$/Vulcan even under neutral conditions, making it promising for efficient charging and lowering

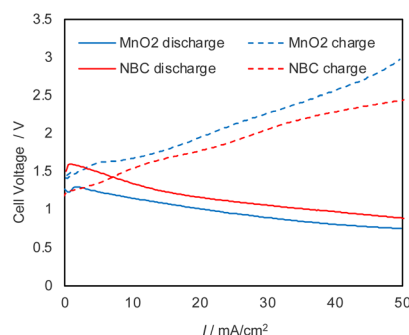**Fig. 7** Charge–discharge polarization curves of Mg–air paper battery cells using NBC (red) and MnO$_2$/Vulcan (blue), respectively.

overpotential. We evaluated the charge–discharge property of the cell using NBC and MnO$_2$/Vulcan as cathode electrocatalyst (Fig. 7). From the polarization curves at charge–discharge, the cell can be charged up to 50 mA cm^{-2}, and the overpotential of the cell using NBC was much lower than that of MnO$_2$/Vulcan.

Only a small number of cycle tests were performed (see ESI, S3†), but it is very important that the cell is not just a single-use disposable for the realization of environmentally friendly batteries.

Conclusions

The paper batteries developed in this study have high output power density and capacity and are also expected to have a low environmental impact after disposal. Metal–air batteries normally use heavy metals, such as manganate compounds, as cathode catalysts for performance, so even if the amount of heavy metal used is small, the battery cannot be disposed of due to the safety and environmental impacts compared with other battery systems. In this study, we showed a primary battery cell, but we also showed a rechargeable battery performance. We believe those primary and rechargeable metal–air paper batteries will contribute to realizing sustainable, lightweight, and high-performance battery systems.

Data availability

The data supporting this article have been included as part of the ESI.†

Author contributions

H. Y. convinced the idea of the work, conducted the whole part of the research, and wrote the whole part of the manuscript. K. I. fabricated carbon alloys, evaluated performance, and fabricated paper battery cells and measured performance.

Conflicts of interest

There are no conflicts to declare.

Acknowledgements

Notes and references

1 T. Juqu, S. C. Willenberg, K. Pokpas and N. Ross, *Adv. Sens. Energy Mater.*, 2022, **1**, 100037.

2 T. H. Nguyen, A. Fraiwan and S. Choi, *Biosens. Bioelectron.*, 2014, **54**, 640–649.

3 M. Hilder, B. Winther-Jensen and N. B. Clark, *J. Power Sources*, 2009, **194**, 1135–1141.

4 A. F. Alharbi, A. A. M. Abahussain, M. H. Nazir and S. Z. J. Zaidi, *Polymers*, 2022, **14**, 1–13.

5 A. Morozan, B. Jousselme and S. Palacin, *Energy Environ. Sci.*, 2011, **4**, 1238–1254.

6 Y. Shao-Horn, W. C. Sheng, S. Chen, P. J. Ferreira, E. F. Holby and D. Morgan, *Top. Catal.*, 2007, **46**, 285–305.

7 E. Fabbri, S. Taylor, A. Rabis, P. Levecque, O. Conrad, R. Kötz and T. J. Schmidt, *ChemCatChem*, 2014, **6**, 1410–1418.

8 M. Shao, A. Peles and K. Shoemaker, *Nano Lett.*, 2011, **11**, 3714–3719.

9 D. W. Kim, O. L. Li and N. Saito, *Phys. Chem. Chem. Phys.*, 2015, **17**, 407–413.

10 K. Qu, Y. Zheng, Y. Jiao, X. Zhang, S. Dai and S. Z. Qiao, *Adv. Energy Mater.*, 2017, **7**, 1602068.

11 M. Antonietti and M. Oschatz, *Adv. Mater.*, 2018, **30**(21), 1706836.

12 M. Grewal, Y. Matsuo and H. Yabu, *New J. Chem.*, 2021, **45**, 19228.

13 X. Zhao, J. Zhu, L. Liang, C. Li, C. Liu, J. Liao and W. Xing, *Appl. Catal., B*, 2014, **154–155**, 177–182.

14 M. Borghei, J. Lehtonen, L. Liu and O. J. Rojas, *Adv. Mater.*, 2018, **30**, 1–27.

15 K. Wang, H. Wang, S. Ji, H. Feng, V. Linkov and R. Wang, *RSC Adv.*, 2013, **3**, 12039–12042.

16 C. Zhao, S. Zhang, M. Han, X. Zhang, Y. Liu, W. Li, C. Chen, G. Wang, H. Zhang and H. Zhao, *ACS Energy Lett.*, 2019, **4**, 377–383.

17 X. Liu, Y. Zhou, W. Zhou, L. Li, S. Huang and S. Chen, *Nanoscale*, 2015, **7**, 6136–6142.

18 H. Yabu, K. Ishibashi, M. S. Grewal, Y. Matsuo, N. Shoji and K. Ito, *Sci. Technol. Adv. Mater.*, 2022, **23**, 31–40.

19 K. Ishibashi, M. S. Grewal, K. Ito, N. Shoji, Y. Matsuo and H. Yabu, *Sci. Technol. Adv. Mater.*, 2022, **2200107**, 31–40.

20 S. Brocato, A. Serov and P. Atanassov, *Electrochim. Acta*, 2013, **87**, 361–365.

21 K. Ishibashi, S. Ono, J. Kamei, K. Ito and H. Yabu, *RSC Appl. Interfaces*, 2024, **1**, 435–442.

22 X. Ao, Y. Ding, G. Nam, L. Soule, P. Jing, B. Zhao, J. Y. Hwang, J. H. Jang, C. Wang and M. Liu, *Small*, 2022, **18**(30), 2203326.